Effect of lattice mismatch on phonon transmission and interface thermal conductance across dissimilar material interfaces

Xiaobo Li and Ronggui Yang*

Department of Mechanical Engineering, University of Colorado, Boulder, Colorado 80309-0427, USA

(Received 5 June 2012; revised manuscript received 15 August 2012; published 27 August 2012)

When phonons transport across a material interface, they experience reflection, transmission, and mode conversion, which results in a local temperature jump at the interface and thus dramatically changes the thermal conductivity of nanostructured materials. Phonon transmission across lattice-matched interfaces has been studied extensively in recent years with the atomistic Green's function (AGF) approach, which usually uses one unit cell to represent the cross section along the interface. However, modeling phonon transmission across realistic material interfaces is much more challenging because realistic interfaces are usually lattice-mismatched ones with atomic reconstruction, defects, and species mixing, which demands a larger cross-sectional area for the AGF simulation. In this paper, an integrated molecular dynamics (MD) and AGF approach is developed to study the phonon transmission across lattice-mismatched interfaces. MD simulation is used to simulate atomic reconstruction close to the interface. The recursive AGF approach is then employed to calculate frequency-dependent phonon transmission across lattice-mismatched interfaces with defects and species mixing, which addresses the numerical challenge in calculating phonon transmission for a relatively large cross-sectional area with reduced computational cost. The study of the relaxed interface formed from two semi-infinite bulk materials shows that lattice mismatch increases the lattice disorder and decreases the adhesion energy, which in turn lowers phonon transmission and reduces the interface thermal conductance across lattice-mismatched interfaces. Low-frequency phonons can be significantly scattered by increasing the defect size across the interface, while high-frequency phonons can be scattered almost completely (phonon transmission < 0.1) across an alloyed layer as thin as 2.27 nm. The effect of lattice mismatch on phonon transmission becomes smaller for interfaces with defects and species mixing. The effect of annealing temperature on the Si/Ge interface thermal conductance was studied. A significant reduction of the Si/Ge interface thermal conductance was observed for a lattice-mismatched interface when annealed at high temperature, which agrees well with the available experimental data in literature.

DOI: 10.1103/PhysRevB.86.054305 PACS number(s): 63.22.−m, 44.10.+i, 68.35.−p, 63.20.kp

I. INTRODUCTION

Interfaces play a critical role in phonon dynamics and thermal conductivity of nanostructured materials.[1–3] When phonons transport across a material interface, they experience reflection, transmission, and mode conversion, which results in a local temperature jump at the interface.[4] Such a temperature jump is described by the interface thermal resistance, thermal boundary resistance (TBR), or Kapitza resistance, owing to Kapitza's original work.[1] With temperature T_1 and T_2 at the two sides of the interface, and heat flux q ($\mathrm{W/m^2}$) flowing across the interface, the thermal boundary resistance (R) can be written as $R = (T_1 - T_2)/q$, and the interface thermal conductance (K) is defined as the inverse of the thermal boundary resistance, $K = 1/R$.

In the past two decades, molecular dynamics (MD) simulations have been employed extensively to study the interface thermal conductance across various material interfaces,[5–13] such as Kr/Ar,[7] Si/In,[11] carbon nanotube/Si,[12] Si/polymer,[9] and PbTe/GeTe.[13] A relatively good understanding of the reduced lattice thermal conductivity in nanostructured materials due to the thermal boundary resistance has been obtained. However, the interface thermal conductance alone from MD simulations, which describes the collective motion of all phonons across an interface and lacks details about how each specific phonon is scattered at the interface, is not sufficient for developing predictive modeling tools for novel nanostructured materials with extraordinary thermal properties. For example, large-scale nano-enabled bulk systems with multiple interfaces such as integrated circuits (ICs)[14] and nanocomposites[15,16] call for a better set of variables and simulation tools to describe such systems. An empirical approach is the Boltzmann transport equation-based (BTE-based) deterministic and stochastic approaches, which could potentially bridge the length scale from a few nanometers to the macroscale.[3,17–21] The knowledge of how a phonon with any specific frequency supported by a material is transmitted, reflected, and converted across a realistic material interface which could have atomic reconstruction, species diffusion, and vacancies is essential for the understanding of the interface thermal conductance, which can be easily calculated using the Landauer formalism,[22] and for developing frequency-dependent BTE-based multiscale design and modeling tools.

Modeling frequency-dependent phonon transmission across material interfaces has been challenging. The acoustic mismatch model (AMM) and diffuse mismatch model (DMM) are often used for the calculation of phonon transmission.[1] AMM considers long-wavelength phonons and uses the acoustic impedances of the materials for the calculation of phonon transmission. The model is strictly valid only at low temperatures. Phonon scattering at interfaces is assumed to be completely diffusive in DMM,[1] which better predicts phonon transmission across rough interfaces. Although AMM and DMM have been used exclusively as inputs for phonon BTE-based thermal conductivity models of nanostructures and for explaining experimental observation of reduced thermal

conductivity in nanostructured materials, neither AMM nor DMM can accurately capture the underlying physics of phonon transport across material interfaces with detailed atomic structures.

Significant progress has been made recently in the study of phonon transmission using atomistic simulation methods, including the phonon wave-packet method[23] based on molecular dynamics simulations, linear lattice dynamics,[24,25] and the atomistic Green's function (AGF) approach, which solves the phonon dynamic equation under harmonic approximation. In particular, the frequency-dependent phonon transmission across a variety of material interfaces has been studied using the AGF approach, such as the interface in low-dimensional atomic chains,[26] strained Si/Ge interfaces,[27] metal/graphene nanoribbon (GNR) interfaces,[28] the rough interface between two face-centered cubic (fcc) crystals,[29] and more recently, across confined material interfaces.[30] However, all the past AGF-based studies on phonon transmission across interfaces[27–32] focused on lattice-matched material interfaces, where the interatomic distance of one material is usually adjusted to match that in the other material in the directions parallel to the interface to simplify the calculations. For example, Si (or Ge) is strained to have the same lattice constant as Ge (or Si) along the interface plane to study phonon transmission across the Si/Ge interface while the interatomic distance in the direction perpendicular to the interface is adjusted according to the Poisson's ratio in Ref. 27. A similar numerical technique has been applied to study the phonon transmission across a TiC/GNR interface in Ref. 28 where the GNR unit cell near the interface is strained to match half of the face diagonal distance of the TiC unit cell. In Ref. 29, two fcc crystals with mass ratio and force constant ratio inherited from Si and Ge are used for the study of phonon transmission across rough interfaces and the lattice constants of the two crystals are adjusted to match each other. In the lattice-matched systems, perfect atomic bonds similar to the ones in their constituent materials are formed at the interface, with no bond breaking or reconstruction, since the interatomic distance is the same for both materials at the interface.

However, realistic material interfaces are usually lattice mismatched. For example, Si and Ge have a 4% mismatch in lattice constants (Si: 5.43 Å and Ge: 5.65 Å). Such lattice mismatch complicates the phonon transport processes across the interface more than that being ideally simulated without lattice mismatch. Pettersson and Mahan[33] were probably the first ones who realized the importance of lattice mismatch on phonon transport across interfaces in the 1990s. By studying phonon transport across unrelaxed lattice-mismatched interfaces formed from model materials with cubic lattices using the lattice dynamics method, they found that: (1) more phonons can be generated when phonons are scattered at the lattice-mismatched interfaces than across lattice-matched ones because of the enhanced phonon mode conversion; (2) the phonon transmission coefficient across lattice-mismatched interfaces is smaller than that across lattice-matched interfaces due to the weakening of bond strength. However, the atomic model system they used was not relaxed. In addition to lattice mismatch, vacancies, defects, and species mixing could all happen in material interfaces due to manufacturing/processing constraints, which could significantly change the phonon scattering at interfaces. There is not much work using either lattice dynamics[25,34] or other methods to study phonon transmission across realistic material interfaces due to the physical and numerical complexity.

In this paper, we develop an integrated atomistic simulation method to study frequency-dependent phonon transmission across lattice-mismatched interfaces with and without defects and species mixing. MD simulation is used first to simulate the relaxed interfacial structure and then the AGF approach is used to simulate the phonon transmission across these relaxed interfaces. Although the AGF approach is relatively easier to implement and is more efficient for the calculation of phonon transmission compared to other methods (such as the lattice dynamics and the wave-packet methods),[30] the computational challenge is still significant for realistic material interfaces. In Sec. II, a recursive AGF method is applied and discussed in detail to address the computational challenges for the phonon transmission calculation across lattice-mismatched interfaces with relatively large cross-sectional area. In Sec. III A, phonon transmission across relaxed interfaces formed from two semi-infinite bulk materials with different percentages of lattice mismatch are studied. In Secs. III B and III C, we compare the calculated phonon transmission across lattice-matched and lattice-mismatched interfaces with defects and species mixing. In Sec. III D, we compare the interface thermal conductance of a Si/Ge interface from our AGF simulations with the ones obtained from experiments and MD simulations. The effect of annealing temperature on the interface thermal conductance was elucidated. Section IV concludes this work.

II. SIMULATION METHODS

Modeling phonon transmission across lattice-mismatched material interfaces with defects and species mixing is challenging because a relatively large cross-sectional area must be used for the AGF simulations. The numerical challenges are analyzed based on a brief introduction of the general AGF approach in Sec. II A. In Sec. II B, the AGF approach with recursive method is discussed in detail to address the numerical challenges in calculating phonon transmission for a relatively large cross-sectional area with reduced computational cost.

A. General AGF approach

Usually periodic boundary conditions need to be applied in atomistic simulations for an infinitely large cross section if there is translational symmetry along the interface directions. Different from the real-space periodic boundary conditions applied in MD simulations, in AGF simulations the periodic boundary conditions can be realized using the wave-vector representation[27] in the momentum space. For a lattice-matched system, the cross section along the interface direction can be as small as one unit cell using the wave-vector representation technique.[27,30] However, a much larger cross section which contains multiple unit cells needs to be used as the basic period for a lattice-mismatched system. For example, 25 unit cells of Si are needed as the basic period along the interface direction for matching the cross-sectional area of the Si/Ge interface so that an infinite-size Si/Ge interface can be formed, considering that there is 4% lattice constant mismatch for Si and Ge. In

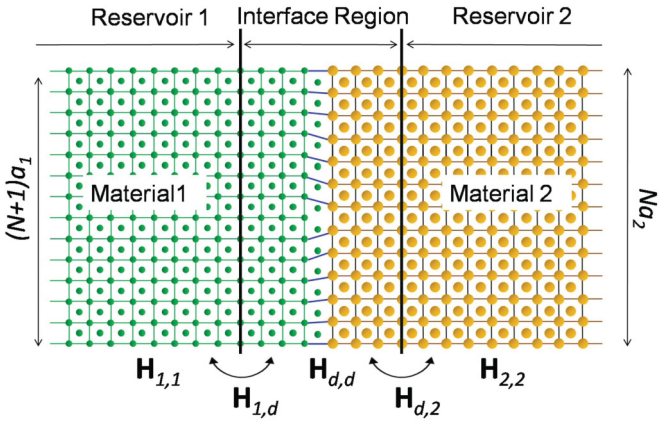

FIG. 1. (Color online) Illustration of a general lattice-mismatched system used in the AGF approach for phonon transmission calculation. With different lattice constants, the smallest period to represent an infinite-size interface in the transverse direction is created by using $N+1$ unit cells in each transverse direction for the materials with smaller lattice constant (a_1) and N unit cells for the one with larger lattice constant (a_2). For a Si/Ge interface, 25 unit cells ($N = 24$) of Si is needed to match the cross section of 24 unit cells of Ge.

addition, the atoms reconstruct near the interfaces of the lattice-mismatched systems. The reconstruction extends to several unit cells away from the interface, which further complicates the computation. In this work, MD simulation under NVE ensemble (constant number of atoms, volume, and energy) is applied to relax the lattice-mismatched interface with atomic reconstruction. The AGF approach is then applied on the reconstructed interface structures to simulate the frequency-dependent phonon transmission across the interfaces.

Figure 1 illustrates a lattice-mismatched atomic system for the calculation of phonon transmission across an interface using the AGF approach. The system consists of three parts: two reservoirs (1 and 2) and the interfacial region. The two reservoirs are semi-infinite regions with bulk material properties. The interfacial region is where phonons transmit, convert, and reflect from reservoir 1 (material 1) to reservoir 2 (material 2).

With force constants obtained under the harmonic approximation, the phonon waves in the lattice system shown in Fig. 1 can be described by the dynamic equation[30]

$$(\omega^2\mathbf{I} - \mathbf{H})\Phi(\omega) = 0, \tag{1}$$

where ω is the angular frequency of lattice vibration (phonons), $\mathbf{H}$ is the harmonic matrix, $\Phi(\omega)$ is the magnitude of the vibrational modes, and $\mathbf{I}$ is the identity matrix. Here bold letters are used to present matrices. In this paper, the harmonic matrix is derived from the Tersoff empirical potential,[35] which predicts reasonably well the mechanical and thermal properties for the Si and Ge materials.[30,36,37]

Instead of solving the dynamical equation directly for the phonon waves as that in the linear lattice dynamics simulations,[24] the atomistic Green's function method is used for obtaining the dynamic response of the lattice system under small perturbation, i.e., small displacement or small force acted on the atoms:

$$(\omega^2\mathbf{I} - \mathbf{H})\mathbf{G} = \mathbf{I}, \tag{2}$$

where $\mathbf{G}$ is the Green's function. The Green's function of the whole lattice system as shown in Fig. 1 can be written in its component form as

$$\mathbf{G} = \begin{bmatrix} \mathbf{G}_{1,1} & \mathbf{G}_{1,d} & \mathbf{G}_{1,2} \\ \mathbf{G}_{d,1} & \mathbf{G}_{d,d} & \mathbf{G}_{d,2} \\ \mathbf{G}_{2,1} & \mathbf{G}_{2,d} & \mathbf{G}_{2,2} \end{bmatrix}, \tag{3}$$

where the subscripts 1, 2, and d correspond to the reservoirs 1, 2, and the interfacial region, respectively. The key for the calculation of phonon transmission across the interfacial region is to find the Green's function $\mathbf{G}_{d,d}$ for the response of the lattice vibration in the interfacial region. $\mathbf{G}_{d,d}$ can be calculated from Eq. (2) through the following matrix inversion by expanding $\mathbf{H}$ and $\mathbf{G}$ in their component forms,[30]

$$\mathbf{G}_{d,d} = [\omega^2\mathbf{I} - \mathbf{H}_{d,d} - \mathbf{\Sigma}_1 - \mathbf{\Sigma}_2]^{-1}, \tag{4}$$

where $\mathbf{H}_{d,d}$ represents the harmonic matrix of the whole interfacial region, as shown in Fig. 1,[30] and $\mathbf{\Sigma}_1$ and $\mathbf{\Sigma}_2$ are the self-energy matrices which represent the energy change to the interfacial region when the reservoirs are connected with the interfacial region. The self-energy matrices $\mathbf{\Sigma}_1$ and $\mathbf{\Sigma}_2$ can be calculated by[27]

$$\mathbf{\Sigma}_1 = \mathbf{H}_{d,1}\mathbf{g}_1\mathbf{H}_{1,d} \tag{5}$$

and

$$\mathbf{\Sigma}_2 = \mathbf{H}_{d,2}\mathbf{g}_2\mathbf{H}_{2,d}, \tag{6}$$

where $\mathbf{H}_{d,1}$, $\mathbf{H}_{1,d}$, $\mathbf{H}_{d,2}$, and $\mathbf{H}_{2,d}$ represent the interactions between the reservoirs and the interfacial region. $\mathbf{g}_1$ and $\mathbf{g}_2$ are the uncoupled Green's functions of reservoirs 1 and 2, respectively, when the reservoirs are disconnected from the interfacial region, and can be written as

$$\mathbf{g}_1 = [(\omega + \delta i)^2\mathbf{I} - \mathbf{H}_{1,1}]^{-1}, \tag{7}$$

$$\mathbf{g}_2 = [(\omega + \delta i)^2\mathbf{I} - \mathbf{H}_{2,2}]^{-1}, \tag{8}$$

where $\mathbf{H}_{1,1}$ and $\mathbf{H}_{2,2}$ are the harmonic matrices of reservoir 1 and 2, respectively. Here a small imaginary number δi is added in Eqs. (7) and (8), which physically represents the broadening of the phonon energy. In practice, finite-sized reservoirs are usually used in numerical simulations to save the computation cost, which induces a discrete phonon density of state (DOS) with finite energy spacing. If there is no phonon energy broadening, the reservoir can behave poorly because the DOS is sharply varying with phonon energy. It is important to choose a value of the δ parameter which is greater than the phonon energy spacing in the finite-sized reservoirs[38] to make the reservoirs well behaved. In calculations, the value of δ is reduced until the converged $\mathbf{g}_1$ and $\mathbf{g}_2$ are obtained. δ is chosen to be 6 orders of magnitude smaller than the phonon frequency in our studies.

With the Green's function $\mathbf{G}_{d,d}$, the total phonon transmission across the interfacial region is then calculated as

$$\Xi(\omega) = \mathrm{Trace}[\mathbf{\Gamma}_1\mathbf{G}_{d,d}\mathbf{\Gamma}_2\mathbf{G}_{d,d}^{+}], \tag{9}$$

where $\mathbf{\Gamma}_1 = i(\mathbf{\Sigma}_1 - \mathbf{\Sigma}_1^{+})$, $\mathbf{\Gamma}_2 = i(\mathbf{\Sigma}_2 - \mathbf{\Sigma}_2^{+})$, and "+" denotes the conjugate transpose of the matrix. Considering that there are multiple phonons at a specific frequency (mode), we use transmission per phonon $\xi(\omega)$ to present our results in

this paper, which is related to the total phonon transmission through

$$\Xi(\omega) = \xi(\omega)M(\omega), \tag{10}$$

where $M(\omega)$ is the total number of phonon modes at frequency ω from material 1. $M(\omega)$ can be calculated from lattice dynamics simulation by counting the number of phonon branches at frequency ω in the phonon dispersion curves. $M(\omega)$ can also be called total phonon transmission in a pure material when the AGF simulation system is set up for the pure material system, since $\xi(\omega)$ equals 1 in a pure material.

In the general AGF method described above, there are two computationally challenging steps for the calculation of phonon transmission in lattice-mismatched systems: (a) calculation of the uncoupled Green's function for semi-infinite reservoirs 1 and 2 with Eqs. (7) and (8), respectively, and (b) solving of Eq. (4) for the Green's function of the interfacial region.

To make sure that the size of the reservoirs is large enough to satisfy the semi-infinite assumption, the decimation technique[39] is usually used to solve Eqs. (7) and (8) instead of direct solutions. However, the efficiency of the decimation technique is still low for the large-size matrix operation in the lattice-mismatched systems. For example, with a cross-sectional area of 25×25 unit cells, which satisfies the minimum size requirement for matching the cross-sectional area of the 4% lattice-mismatched Si/Ge interface, a square matrix (A) with a size twice (to keep the periodicity, A includes both the dynamic matrices of the unit cell itself and the interactions between the neighboring unit cells) of $25 \times 25 \times 8 \times 3 = 15\,000$ (8 atoms per unit cell and 3 degrees of freedom) needs to be constructed in the decimation technique. An iterative procedure is used to solve the uncoupled Green's function ($\mathbf{g}_1$ and $\mathbf{g}_2$) by increasing the size of the reservoirs until the converged $\mathbf{g}_1$ and $\mathbf{g}_2$ are obtained.[39] In this solution procedure, the inverse of A is used to solve the Green's functions. Although A is a sparse matrix, the inverse of A is a full matrix, which demands a large amount of memory (~6 GB). The matrix operation is computationally prohibitive even if the iterative solving procedure is applied in decimation technique. In order to reduce the computational cost, we use the recursive AGF method[40] in this paper, which calculates the response of the whole system from the responses of separated subsystems and uses matrices only 1/4 size of the ones in decimation technique for the calculations (the details will be discussed shortly in Sec. II B). For example, for a simulated system with cross-sectional area of 9 unit cells, our method is about 13 times faster than the decimation technique.

A relatively thick interfacial region needs to be considered in the lattice-mismatched systems, which results in significant challenges in solving Eq. (4). The atomic reconstruction extends the interfacial region to be many layers of atoms rather than a sharp interface with 1–2 atomic layers. For example, if the interfacial region has a thickness of 5 unit cells, the square matrix corresponding to the interfacial region used in solving the Green's function in Eq. (4) is a sparse matrix with a size of about 75,000 and a bandwidth of about 15,000, which demands a large amount of memory and high computational cost for obtaining the inverse of the matrix. Instead of solving Eq. (4), we can again use the recursive method based on matrices with reduced size and bandwidth.

B. AGF approach with recursive method

One great advantage of using the AGF approach to calculate phonon transmission is that the response of the whole system can be calculated from the responses of separated subsystems. Assuming that separated subsystems have an uncoupled Green's function $\mathbf{G}^0$, the response $\mathbf{G}$ of the whole system can be calculated by treating the interactions $\mathbf{V}$ between the subsystems as small perturbations[41] using the Dyson equation,[40]

$$\mathbf{G} = \mathbf{G}^0 + \mathbf{G}^0\mathbf{V}\mathbf{G}. \tag{11}$$

As mentioned in Sec. II A, the challenges in the calculation of the phonon transmission across lattice-mismatched interfaces are due to the computation-costly, large-size matrix operation. Application of the Dyson equation by obtaining the Green's function of a whole system based on divided subsystems with reduced size using the recursive method can greatly reduce the size of the matrix and thus reduce the computational cost.

Figure 2(a) illustrates the detailed procedure of recursive method for calculation of the coupled Green's function. For the systems studied in this paper, we can divide the system into layered structures as subsystems, as shown in step 1 in Fig. 2(a). The separated layers can then be connected together one by one using the Dyson equation, if the division of layers ensures that the interaction extends to the nearest-neighboring layers only. For the lattice system studied, such a criterion is essentially governed by the cutoff distance of the potential function used. Since the cutoff distance of the Tersoff potential for Si and Ge used in this study is about one unit cell,[35] the layer thickness can be as small as half a unit cell along the Z direction in the reservoirs. In the interfacial region, although the atomic interactions are different from those in the reservoirs due to the reconstruction, we can still divide the whole interfacial region into separated layers for the calculations of Green's functions using the recursive method. The thickness of each layer is determined by searching the atoms that have interactions with the atoms at the other end across the layer, but with the largest distance. In order to apply the recursive method, the uncoupled Green's function of each divided layer needs to be calculated first, as shown in step 2 in Fig. 2(a). For the layers in the reservoir, the uncoupled Green's function is obtained using

$$[(\omega + \delta i)^2\mathbf{I} - \mathbf{H}_{j,j}]\mathbf{G}^0_{j,j} = \mathbf{I}, \tag{12}$$

where $\mathbf{H}_{j,j}$ is the harmonic matrix for each divided layer and a small imaginary number δi is added for the calculation of the uncoupled Green's function $\mathbf{G}^0_{j,j}$ for the same reason as discussed with regard to Eqs. (7) and (8). In each reservoir, each unit cell is divided into two layers. Equation (12) only needs to be solved twice for these two distinguishable layers. In the interfacial region, the uncoupled Green's function $\mathbf{G}^0_{k,k}$ is calculated from the harmonic matrix $\mathbf{H}_{k,k}$ for each divided layer k,

$$(\omega^2\mathbf{I} - \mathbf{H}_{k,k})\mathbf{G}^0_{k,k} = \mathbf{I}, \tag{13}$$

which needs to be solved for all the layers.

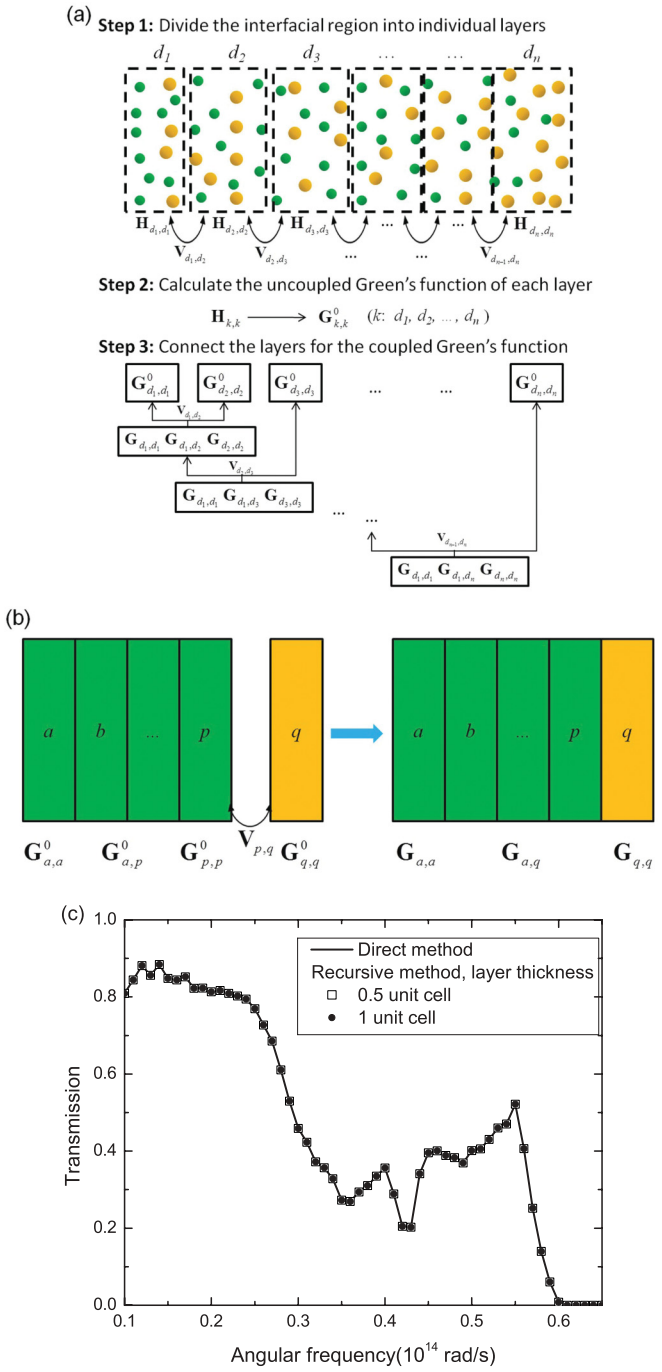

FIG. 2. (Color online) (a) Illustration of the recursive method. The interfacial region is first divided into separated layers. The uncoupled Green's function of each separated layer is calculated. The separated layers are then connected in sequence for the calculation of the coupled Green's function. (b) Detailed calculation of the coupled Green's function after adding a layer in step 3 as shown in (a). In general, assuming that layers a–p have already been connected together, we add another layer q to the system through the interaction $\mathbf{V}_{p,q}$ between layer p and q. Since $\mathbf{G}_{d_1,d_n}$ are needed for the phonon transmission calculation, only the Green's functions related to the first and last layer are recorded for the next step calculation. (c) Verification of the recursive method through the calculation of phonon transmission across the Si/Ge lattice-matched interface. The same results are obtained from the direct method and the recursive method with the thicknesses of the divided layers at 0.5 and 1 unit cell.

The coupled Green's function in the reservoirs and the interfacial region can then be calculated using the Dyson equation. Since only the nearest-neighboring layers have interactions, any two neighboring layers can be connected together first without involving a third layer based on Eq. (11) for the calculation of the coupled Green's functions. Using this method, the divided layers can be connected together in sequence, and only the Green's functions corresponding to the first and last layer are recorded for the next step calculations as illustrated in step 3 in Fig. 2(a). Figure 2(b) shows the detailed calculation of the coupled Green's function after adding a layer. Assuming that layers a–p have been already connected together and the Green's functions recorded for the next step calculation are $\mathbf{G}^0_{a,a}$, $\mathbf{G}^0_{a,p}$, and $\mathbf{G}^0_{p,p}$, we can now add another layer q to the system. With the uncoupled Green's function $\mathbf{G}^0_{q,q}$ of layer q and the interaction $\mathbf{V}_{p,q}$ between layers p and q, the coupled Green's functions ($\mathbf{G}_{a,a}$, $\mathbf{G}_{a,q}$, and $\mathbf{G}_{q,q}$) for the connected layer a–q can be solved through the following equations, which are the component forms of Eq. (11):

$$\begin{aligned}
\mathbf{G}_{a,a} &= \mathbf{G}^0_{a,a} + \mathbf{G}^0_{a,p}\mathbf{V}_{p,q}\mathbf{G}_{q,a},\\
\mathbf{G}_{a,q} &= \mathbf{G}^0_{a,p}\mathbf{V}_{p,q}\mathbf{G}_{q,q},\\
\mathbf{G}_{q,q} &= \mathbf{G}^0_{q,q} + \mathbf{G}^0_{q,q}\mathbf{V}_{q,p}\mathbf{G}_{p,q},\\
\mathbf{G}_{p,q} &= \mathbf{G}^0_{p,p}\mathbf{V}_{p,q}\mathbf{G}_{q,q},
\end{aligned} \tag{14}$$

where $\mathbf{V}_{q,p} = \mathbf{V}^+_{p,q}$, $\mathbf{G}_{q,a} = \mathbf{G}^+_{a,q}$. In the equations set (14) above, the equation for $G_{p,q}$ is added to make the set of equations complete, but not recorded for the next step calculation. The coupled Green's functions ($\mathbf{G}_{a,a}$, $\mathbf{G}_{a,q}$, and $\mathbf{G}_{q,q}$) are then used for the next step calculation. The whole system, including the reservoirs and the interfacial region, can be connected in such a manner to calculate the coupled Green's function in the interfacial region for the phonon transmission.

The phonon transmission across the interfacial region can then be calculated from the response (or the Green's function) between the first and last layer without knowing the Green's function of the whole interfacial region, which significantly reduces the computational cost by using the recursive method. Assuming the first and the last layer in the interfacial region are layers d_1 and d_n, the total phonon transmission is then calculated as

$$\Xi(\omega) = Tr[\mathbf{\Gamma}_{1(d_1,d_1)}\mathbf{G}_{(d_1,d_n)}\mathbf{\Gamma}_{2(d_n,d_n)}\mathbf{G}^+_{(d_1,d_n)}], \tag{15}$$

where $\mathbf{G}_{(d_1,d_n)}$ is the Green's function corresponding to the first and last layer in the interfacial region, $\mathbf{\Gamma}_{1(d_1,d_1)} = i(\mathbf{\Sigma}_{1(d_1,d_1)} - \mathbf{\Sigma}^+_{1(d_1,d_1)})$, and $\mathbf{\Gamma}_{2(d_n,d_n)} = i(\mathbf{\Sigma}_{2(d_n,d_n)} - \mathbf{\Sigma}^+_{2(d_n,d_n)})$. $\mathbf{\Sigma}_{1(d_1,d_1)}$ and $\mathbf{\Sigma}_{2(d_n,d_n)}$ are the submatrices in the self-energy $\mathbf{\Sigma}_1$ and $\mathbf{\Sigma}_2$ corresponding to the layer d_1 and d_n (the first and last layer in the interfacial region).

The division of the layers in the recursive method is not unique as long as it meets the division rule: the interaction extends to the nearest-neighboring layers only. Figure 2(c) verified that the recursive method with different thicknesses of divided layers gives exactly the same phonon transmission results as those from the direct method, when this method is applied for the calculation of phonon transmission across a lattice-matched Si/Ge-like interface.

Using the Landauer formalism, the thermal conductance K can then be easily calculated with the obtained total phonon

transmission,[22]

$$K = \frac{J}{\Delta T} = \frac{1}{2\pi S}\int_0^\infty d\omega\hbar\omega\frac{\partial f(\omega,T)}{\partial T}\Xi(\omega), \qquad (16)$$

where S is the cross-sectional area perpendicular to the heat flow direction, $f(\omega,T)$ is the phonon occupation number, and T is temperature. Within the linear response regime, the calculation using Eq. (16) is performed in the limit of infinitely small temperature difference.

We shall note that harmonic approximation is assumed in the above description of the AGF approach for the calculation of phonon transmission. In principle, the anharmonicity could also be included in the AGF approach, as shown in the few recent studies on low-dimensional systems, where the Feynman diagram is used to consider the multiple-phonon scattering process due to the anharmonic force constants at the interfacial region.[42,43] However, this method has not been applied for more complex systems due to the computational challenges. The recursive method described in this paper can potentially be used to solve some of the computational challenges. Similar to MD, another significant limitation of the AGF approach is the availability of the empirical potential for materials and the accuracy of the empirical potentials. Although there have been significant efforts in developing empirical potentials for materials of interest, the empirical potential for a large number of materials and interfaces is not available. The recent work on obtaining the force constants of crystals from the first-principles calculations[44,45] can significantly expand the power of the AGF method, although there might be challenges to obtaining force constants across material interfaces using the first-principles calculations.

III. RESULTS AND DISCUSSION

The effects of lattice mismatch on frequency-dependent phonon transmission across Si/Ge-like material interfaces are presented in this section. We start with the relaxed interfaces formed between two semi-infinite bulk materials with different percentages of lattice mismatch in Sec. III A. Sections III B and III C present the results for lattice-mismatched interfaces with defects and species mixing. Finally, in Sec. III D we compare the interface thermal conductance of a Si/Ge interface predicted using AGF simulations with those from experiments and MD simulations.

A. Relaxed interface formed between two semi-infinite bulk materials

In this study, Ge with the Tersoff empirical potential is modified to create new Ge-like materials with different lattice constants so that the relaxed interfaces with different percentage of lattice mismatch can be formed between semi-infinite bulk Si and Ge-like materials to systematically study the effect of lattice mismatch on phonon transmission. Modification of the Tersoff empirical potential for Ge-like materials is shown in detail in the Appendix. Si is used as material 1 and Ge-like material is used as material 2, as shown in Fig. 1. The interface is formed by connecting the (1 0 0) plane of the two materials together with the distance calculated from the average nearest-plane distance of the two materials. The cross-sectional area for the basic period is determined by the percentage of lattice mismatch with the detailed parameters listed in Table I. Ten unit cells are used for the length in the Z direction (heat-transport direction) for each material, which is sufficiently long that the atomic reconstruction near the interface is not affected by the choice of a larger length. Initially, the constructed structure has a large strain at the interface due to the lattice mismatch. MD simulations under a constant pressure (0 Pa) and a constant temperature (300 K) are performed to relax the structure until the potential energy of the system reaches its minimum.

TABLE I. Lattice constant and the size of the cross-sectional area (N unit cell in each transverse direction) of Ge or Ge-like materials for the structure shown in Fig. 1 with different percentages of lattice mismatch. The percentage of lattice mismatch of the Si/Ge system is 4.2%.

Percentage of lattice mismatch	N	Lattice constant of Ge or Ge-like (Å)
4.2%	24	5.6729
5.6%	18	5.7486
8.3%	12	5.8998
16.7%	6	6.3537

Figures 3(a) and 3(b) show part of the cross section (perpendicular to the interface) of the interfacial structures of the Si/Ge-like system with an 8% lattice mismatch before and after the system is relaxed. In Fig. 3(a), the two materials with their original bulk lattice structures are brought together into contact. After relaxation, the atoms over several unit cells across the interface are redistributed so that they slightly deviate from their equilibrium position due to the lattice mismatch, as shown in Fig. 3(b). Figure 3(c) shows the reconstructed interface of the Ge-like material (the leftmost atomic plane of the Ge-like material). The atoms with large displacements concentrate mainly in areas around the dashed lines, as shown in the figure. The dashed line appears to be the longest path, which involves the largest number of atoms in the structure for energy minimization due to the periodic boundary condition used in the transverse directions.

Figure 4(a) shows the frequency-dependent phonon transmission per phonon across the relaxed interfaces with different percentages of lattice mismatch. The transmission of low-frequency phonons from Si to Ge-like materials has a relatively large value due to the larger DOS of low-frequency phonons in Ge-like material than that in Si.[30] It is interesting to note that even though there are multiple phonons in the Ge-like material side to closely match a similar frequency phonon from the Si side, the transmission is still less than 1 (about 0.85). This is due to the mismatch of phonon spectra. After all, the frequency and wave vector of phonons supported by the two materials at different sides of the interface are always different and can never find a perfect match for any specific phonons.

When a low-frequency phonon transmits from Si to Ge-like materials, there can be multiple phonons in the Ge-like material side with similar frequency to match the incoming phonons from the Si side. In contrast, the phonon transmission at low

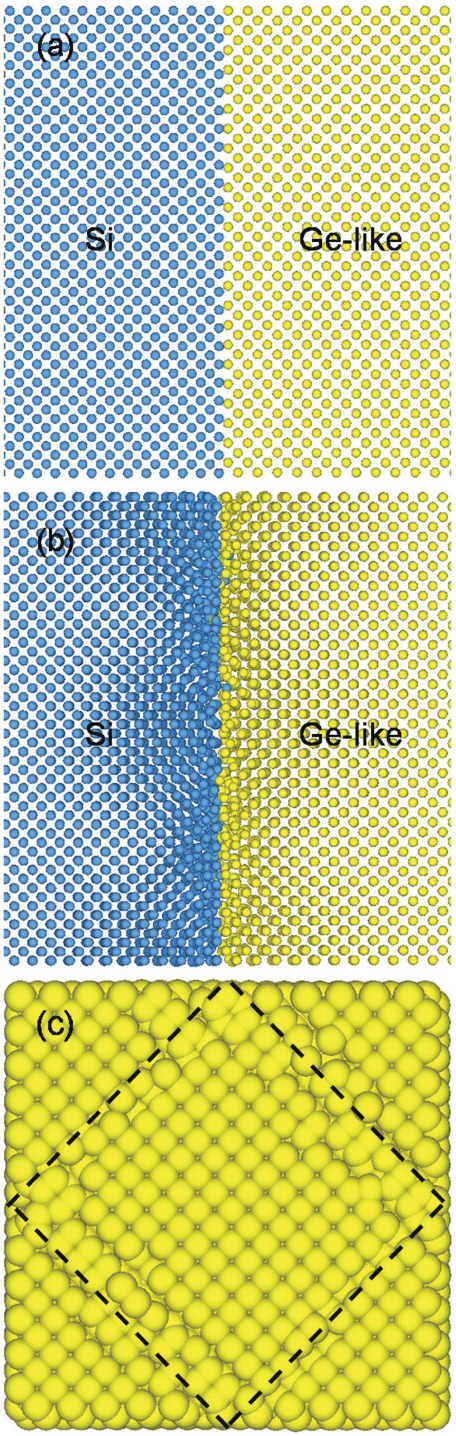

FIG. 3. (Color online) Relaxed interfaces formed between Si and Ge-like materials with an 8% lattice mismatch: (a) the initial structure, (b) the structure after relaxation with MD simulation, and (c) the reconstructed interface of the Ge-like material (the leftmost atomic plane of the Ge-like material).

frequency from Ge-like to Si will be much smaller (about 0.45, not shown here), due to the much fewer phonons at similar frequencies available in the Si side to match those from the Ge-like materials side.[25,30]

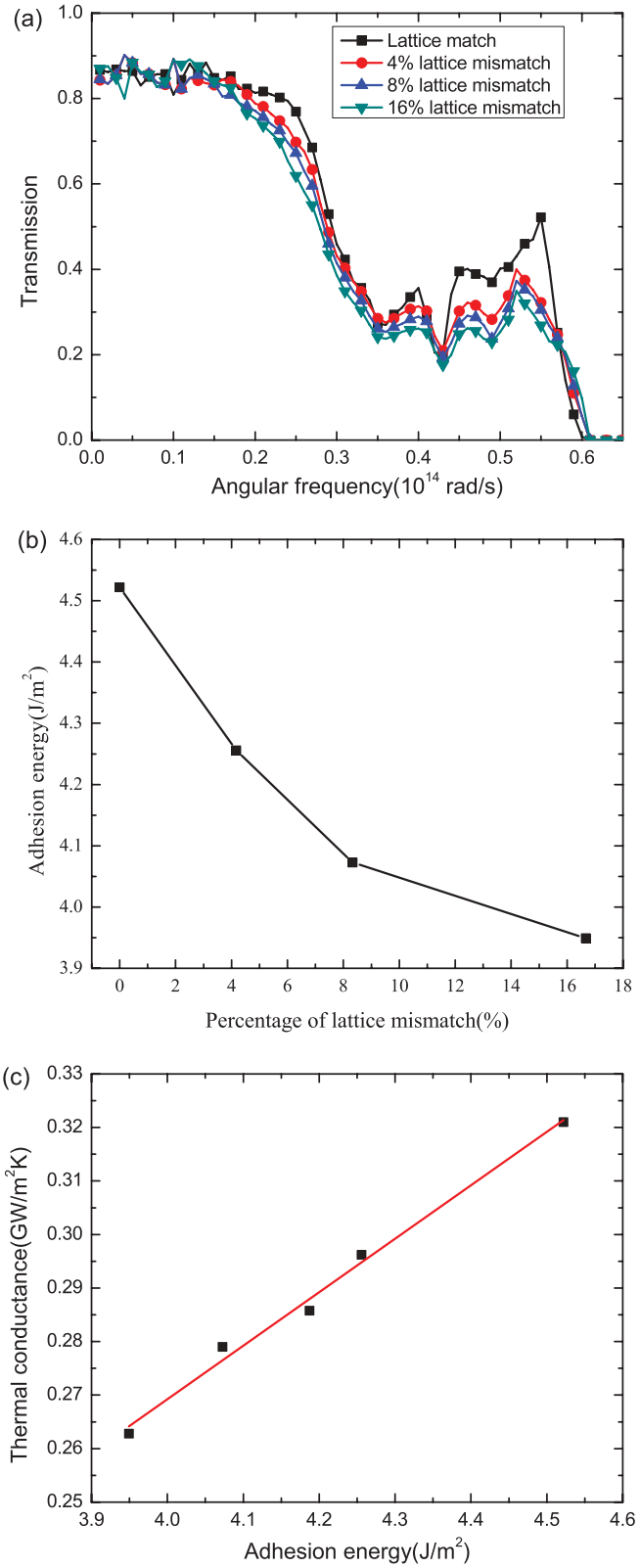

FIG. 4. (Color online) (a) Frequency-dependent phonon transmission across the relaxed interfaces formed between Si and Ge-like material with different percentages of lattice mismatch. (b) Adhesion energy of the relaxed interface as a function of different percentages of lattice mismatch. (c) The thermal conductance as a function of the interface adhesion energy.

Figure 4(a) clearly shows that phonon transmission decreases with the increasing percentage of lattice mismatch. Phonon transmission across the relaxed lattice-mismatched interfaces is affected by several factors. Phonon mode conversion would probably increase with the inclusion of lattice mismatch, which essentially increases the phonon transmission.[33] However, the atomic disorder at the interface after relaxation decreases the phonon transmission. The larger the lattice mismatch, the higher the atomic disorder. Such a competition results in reduced phonon transmission with the increase of lattice mismatch.

When an interface is formed from two materials, energy will be released due to the formation of atomic bonds, which is defined as the adhesion energy, $\Delta E = E_1 + E_2 - E_{12}$ with E_1 and E_2 as the energy of the bulk material 1 and 2 before the formation of the interface and E_{12} as the energy of the relaxed interface system. Figure 4(b) shows that the adhesion energy decreases with the increasing percentage of lattice mismatch. With the increase of lattice match, the atomic disorder increases, which results in higher energy (E_{12}) of the system due to higher residual strains across the lattice-mismatched interface. It is interesting to correlate the interface thermal conductance as a function of the adhesion energy as shown in Fig. 4(c). The interface thermal conductance deceases linearly as the adhesion energy decreases across the lattice-mismatched interface.

B. Interfaces with vacancy defects

Vacancies around an interface can greatly affect the phonon transmission and interface thermal conductance. In this section, we consider Si/Ge-like material interfaces with spherical vacancy defects at fixed lattice mismatch of 8%. In this study, the centers of the spherical vacancy defects are randomly distributed in the two atomic layers near the interface (one layer from Si and the other layer from the Ge-like material). We can then characterize the vacancy defects at an interface with two parameters: defect size (d) and defect density (f). Initially, the vacancy defects are formed by removing atoms within a radius of $d/2$ around the spherical defect centers. The total number of defects created is calculated from the defect density and the total number of atoms in the two atomic layers near the interface. The structure is then relaxed by performing MD simulation under NVE ensemble with average temperature at 300 K and average pressure at 0 Pa. Figures 5(a) and 5(b) show the initial and final structure of the defected interface (Ge-like material side) with a defect size of 0.6 nm (about 40 atoms per vacancy) and defect density of 3%. Atomic reconstruction occurs at the interface due to both the formation of vacancy defects and the lattice mismatch. However, the size of the defects remains the same as the one before relaxation. In other words, no diffusion of such large vacancy defects into smaller ones was observed, as otherwise would be for real material interfaces. This is likely due to the low-temperature MD relaxation process that cannot capture the real physics, which is not the focus of this paper. We also note that the large vacancy defects at the interfaces can also be viewed as interface roughness. Nevertheless, this study can be viewed as an idealized model to study the scattering of phonons at the interface due to the characteristic size change of scattering centers.

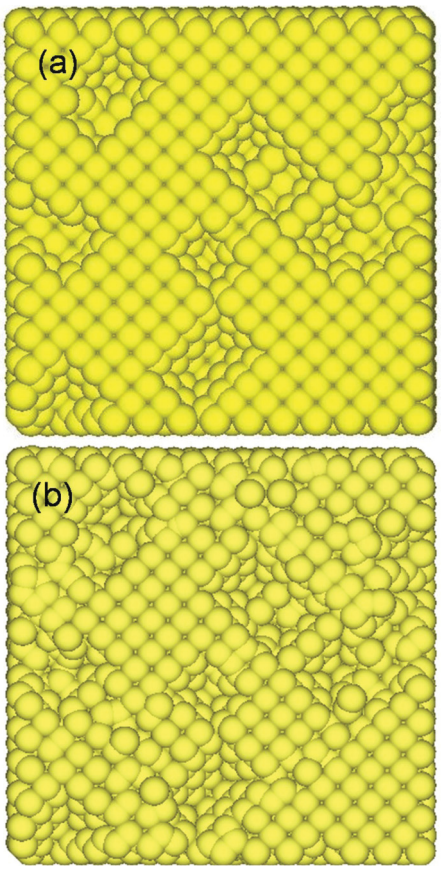

FIG. 5. (Color online) (a) Initial structure, and (b) final structure after MD relaxation, of the interface with defect size of 0.6 nm and defect density of 3%.

Figure 6(a) shows the frequency-dependent phonon transmission as a function of defect density when the vacancy defect size is kept at one-atom size. The phonon transmission decreases only slightly with increasing defect density, especially when the defect density is low. The phonon-defect scattering greatly depends on the phonon wavelength and the defect size. With a very small one-atom defect size d considered here, which is much smaller than the phonon wavelength λ (the smallest phonon wavelength is twice that of the nearest atomic plane distance), the phonons experience Rayleigh scattering, where the scattering cross section can be written as $\sigma \sim d^6/\lambda^4$.[46] At low defect density, such one-atom-size defects do not scatter strongly and frequently with phonons, which results in only slight decrease of the phonon transmission. Earlier MD simulation work reported slightly affected interface thermal conductance with point vacancies at a density of 1%, which also indicates that phonon transmission changes only slightly at low defect density when defect size is small.[8]

Figure 6(b) shows that phonon transmission decreases when the defect size is increased from one atom to 0.6 nm when the defect density is fixed at 3%. The defect size changes the transmission of low-frequency phonons remarkably compared to the effect of defect density when the defects are in the size of only one atom in Fig. 6(a). This is because the phonons with longer wavelength (or lower frequency) comparable to the defect size are strongly scattered when the defect

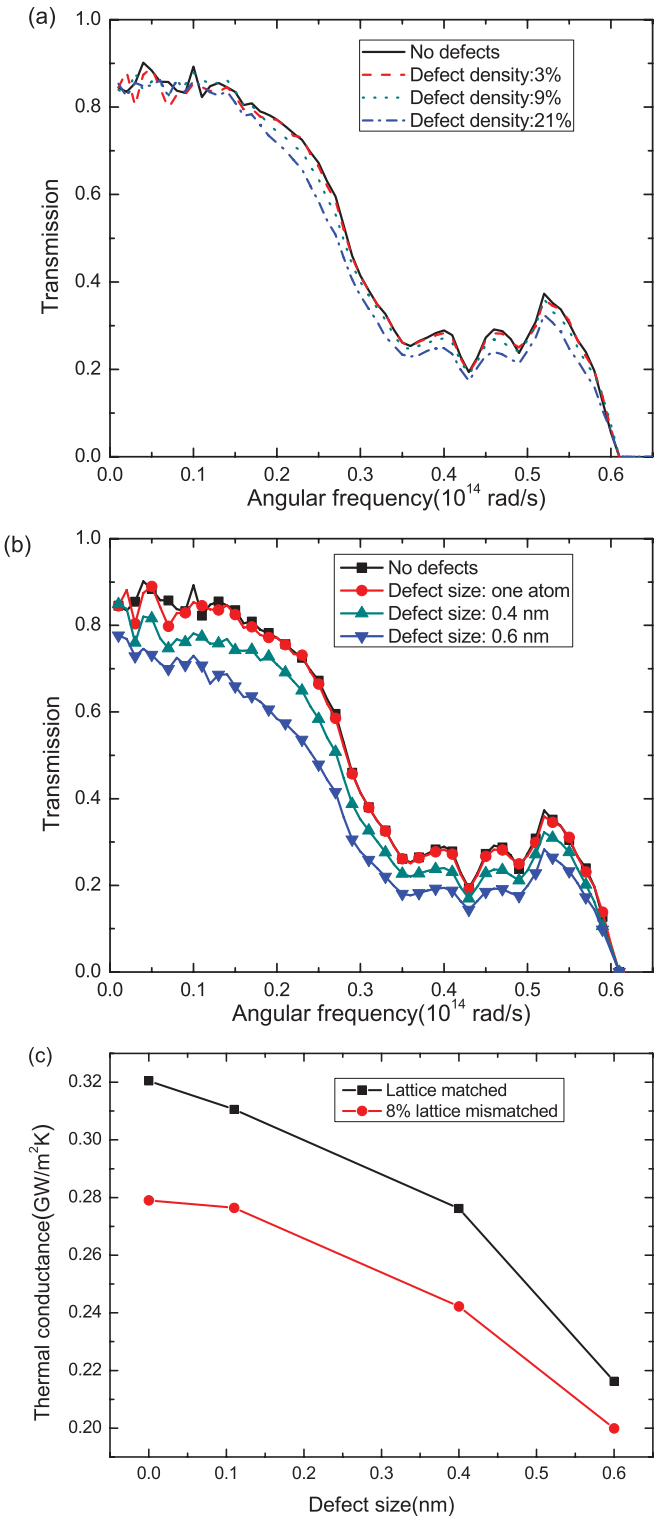

FIG. 6. (Color online) Phonon transmission across 8% lattice-mismatched interface with (a) different defect density when defect size is kept at one atom and (b) different defect size when defect density is kept at 3%. (c) Thermal conductance with different defect size and fixed defect density at 3% for both lattice-matched and 8% lattice-mismatched interface.

size increases. Figure 6(c) compares the interface thermal conductance across the lattice-matched and lattice-mismatched interfaces (8% lattice mismatch to Si) with varying defect size at a fixed defect density of 3%. The difference in the interface thermal conductance decreases between the lattice-matched and lattice-mismatch interfaces when the defect size increases. With the increasing defect size, the phonon transmission is more affected by the defect than the lattice mismatch.

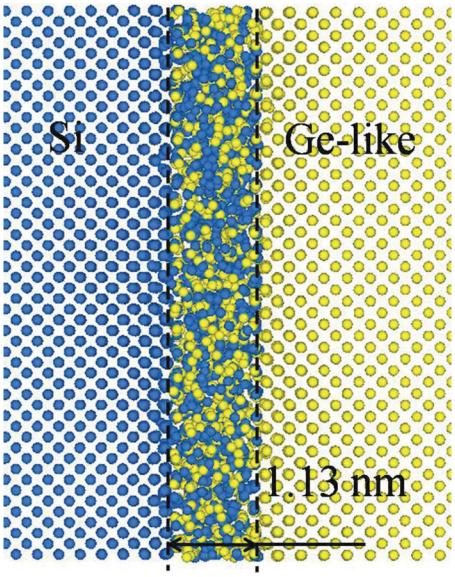

FIG. 7. (Color online) The alloyed Si/Ge-like interface structure with thickness L of 1.13 nm. The percentage of lattice mismatch between Si and Ge-like material is 8%. The alloyed interface is formed by locally melting the region at 4000 K and quenched at 300 K using MD simulation.

C. Alloyed interface

Species can diffuse into each other at material interfaces, especially under high temperature and after extended time. In this section, phonon transmission across alloyed interfaces with an 8% lattice mismatch is studied. MD simulations are conducted to form the alloyed interfaces. The lattice-mismatched interface is constructed first by connecting the semi-infinite Si and Ge-like materials. The section with a thickness L near the interface (half from each material) is then melted locally at 4000 K and quenched at 300 K to form the alloyed interface using MD simulation under an NVE ensemble for each process. Figure 7 shows one of the alloyed Si/Ge-like interface structures with $L = 1.13$ nm. Si and Ge-like atoms at the interface within the 1.13-nm region are fully mixed and form an amorphous layer. The calculation results for the frequency-dependent phonon transmission presented below are for the interface section that includes both the $L = 1.13$ nm, totally mixed region and the distorted lattice nearby.

Figure 8(a) shows the frequency-dependent phonon transmission across the alloyed interface with varying thickness L. Phonon transmission decreases only slightly across a 0.28-nm alloyed layer. Similar to the scattering of phonons across interfaces with point vacancy defects presented in Sec. III B, 0.28 nm of the alloyed layer is far too thin to scatter phonons with longer wavelength than the alloyed layer thickness. With the increase of the alloyed layer thickness,

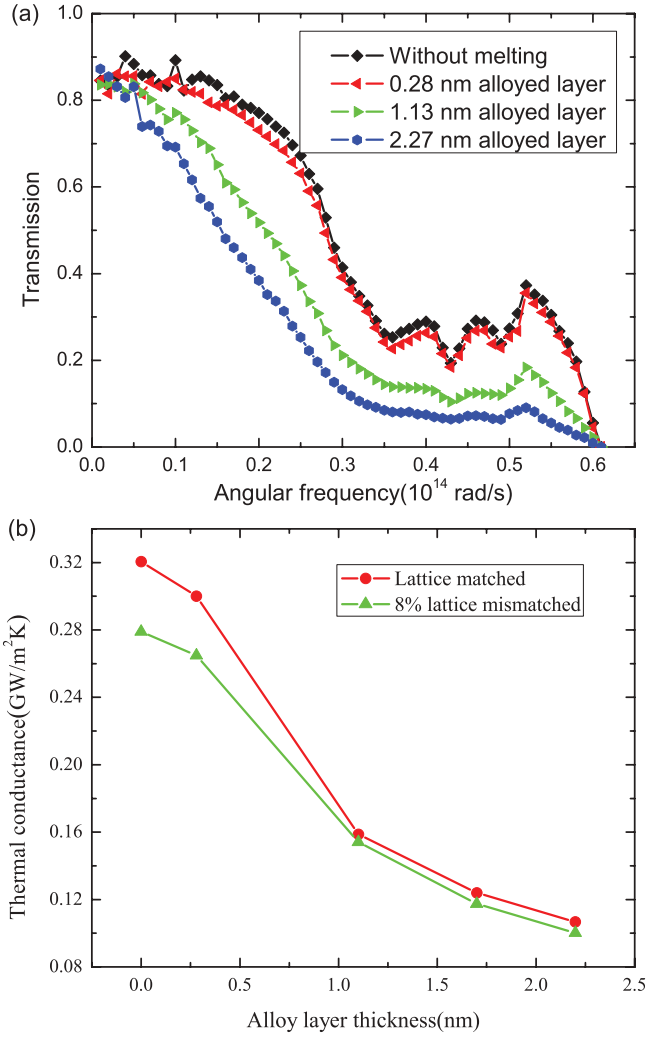

FIG. 8. (Color online) (a) Phonon transmission across an alloyed Si/Ge-like lattice-mismatched interface with different alloyed layer thickness. (b) Interface thermal conductance across alloyed Si/Ge-like lattice-mismatched and lattice-matched interfaces with different alloyed layer thickness. The result without melting is the one across the relaxed interface formed from two semi-infinite bulk materials.

the transmission of high-frequency phonons can be reduced to a very low value. For example, the phonon transmission across a 2.27-nm alloyed interface layer is below 0.1 for the phonon frequency ranging from around 0.3×10^{14} to 0.6×10^{14} rad/s. With the same alloyed interface layer thickness, the low-frequency phonons have a relatively large phonon transmission value (>0.5 for phonon frequencies lower than 0.15×10^{14} rad/s), which is due to the low scattering rate for the long-wavelength phonons at the small scattering centers in the alloyed layer. As the layer thickness increases, the peaks in the phonon transmission disappear, due to the loss of the original momentum and random traveling directions of the phonons after scattering within a thick alloyed layer, i.e., strong mode conversion of the phonons across the alloyed layer.

Figure 8(b) compares the interface thermal conductance across both the lattice-matched and lattice-mismatched interface (8% lattice mismatch to Si) with species mixing. The effect of lattice mismatch on the change of phonon transmission becomes small with increasing alloyed layer thickness due to the random phonon scattering across the alloyed layer. For the lattice-mismatched interface, the interface thermal conductance is 0.1 GW/m^2 K across a 2.27-nm alloyed layer. The thermal conductivity of the Si-Ge alloy formed in the interfacial region ($Si_{0.54}Ge_{0.46}$) is about 10 W/mK.[47] The thermal conductance of the 2.27-nm alloy layer itself is estimated to be ~4.4 GW/m^2 K, which is significantly larger than the overall thermal conductance from our calculation. This indicates that the interface thermal resistance across the alloyed interface is mainly governed by the adjacent regions between the bulk materials and the alloyed layer, where atoms slightly deviate from their original position in a bulk crystal. The reduction of interface thermal conductance due to species mixing has also been reported experimentally.[48,49] For example, the measured interface thermal conductance across a C/TiN interface decreases from 0.2 GW/m^2 K to 0.084 GW/m^2 K after anealing at high temperature,[49] which can clearly be explained as the effect of species diffusion at the interface after annealing. Reduced interface thermal conductance across Cr/Si interfaces with species mixing was reported in Ref. 48.

D. Interface thermal conductance of Si/Ge interface

Figure 9 shows the comparison of the interface thermal conductance of the Si/Ge interface obtained from different simulation methods and extracted from experiments. The interface thermal conductance across a strained lattice-matched Si/Ge interface is calculated using nonequilibrium MD (NEMD) simulation following the direct method for the calculation of interface thermal conductance in Ref. 10. The average lattice constant of Si and Ge along the interface direction is used

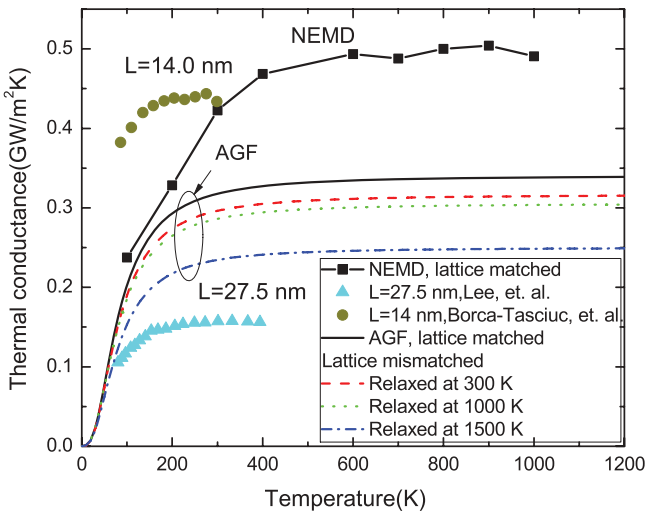

FIG. 9. (Color online) Comparison of the interface thermal conductance of the Si/Ge interface from our AGF simulation with the results from experiments and MD simulations. The value from experiments is extracted from measurement of thermal conductivity of the superlattice described in Refs. 50 and 51. The NEMD simulation is on the strained lattice-matched Si/Ge interface. AGF simulations have been performed based on the structures annealed at different temperatures for both lattice-matched and lattice-mismatched Si/Ge interfaces.

to form the interface and the average stress perpendicular to the interface direction is relaxed to zero. Similar to other reported studies, the calculated interface thermal conductance greatly depends on the simulation domain length of Si and Ge, and eventually it converges with a length greater than 100 unit cells. The converged value is plotted in Fig. 9 for comparison. The interface thermal conductance calculated using AGF agrees reasonably well with the NEMD results at low temperature (100 K) and the discrepancy becomes evident with increasing temperature. This could be due to the fact that AGF simulations are based on the harmonic approximation and do not consider the inelastic phonon scattering while the MD simulation considers inelastic phonon scattering. This also points to the importance of including anharmonic terms for the future development of the AGF approach.

To best of our knowledge, direct measurement of the interface thermal conductance of a single Si/Ge interface is not available. However, we can extract the values from superlattices by assuming that the measured thermal resistance of superlattices[50,51] is a series resistance of interface thermal resistance and intrinsic layer resistance. With small superlattice period thickness ($3 \sim 6.5$ nm in Ref. 50 and 4.4 nm in Ref. 51), the interface thermal conductance extracted from experiments[50,51] is about 4–8 times larger than the results from NEMD and AGF simulations. With a larger period thickness (27.5 nm in Ref. 50 and 14 nm in Ref. 51), the experimental results are about 0.3–1.5 times the simulation results as plotted in Fig. 9, which can be regarded as reasonable agreement since our calculations are on interfaces formed from two perfect bulk materials and should be compared with larger period thickness. The larger experimental results of interface thermal conductance with small period thickness could be attributed to the coherent phonon transport in the superlattice and deserves further study.[52]

Si/Ge Superlattices are expitaxially grown at a relatively high temperature, i.e., about 1000 K in Ref. 50, which can induce atomic reconstruction in the lattice-mismatched Si/Ge interfaces. We thus anneal the Si/Ge interface at a different temperature and then bring the temperature back to 300 K for the AGF calculation of phonon transmission and the interface thermal conductance. In the annealing process, the temperature of the whole system is elevated to the target value and the system is kept at this high temperature and zero pressure until the potential energy of the system becomes stable. The system is then cooled to 300 K at a cooling rate of 1 K/ps by rescaling the system temperature. As expected, the interface thermal conductance for the lattice-matched interface is found not to vary with the annealing temperature up to 1500 K, because there is essentially no atomic reconstruction across the lattice-matched interface with perfect bonding. For the lattice-mismatched interface, there is about 6.8% reduction in interface thermal conductance at 300 K if the system is relaxed at 300 K compared with the results for the lattice-matched interface. Another 3% reduction is observed if the annealing temperature is increased to 1000 K. However, a much larger decrease of interface thermal conductance is observed if the annealing temperature is further increased to 1500 K, due to the significant increase in the atomic disorder observed in the interfacial structure. Such numerical results on the reduced interface thermal conductance across the lattice-mismatched interface under high-temperature annealing could possibly explain the lower experimental value of interface thermal conductance of the Si/Ge interface extracted from superlattice experiments than that of the theoretical calculations. Literature also suggests that an alloyed Si-Ge layer can form across the Si/Ge interface during the epitaxial growth process at high temperature because atoms with high velocity could knock off the ones on the substrate.[53] Our simulation in Sec. III C shows that the thermal conductance of the Si/Ge interface can be further lowered if an alloyed interface is formed, which can be another important reason to explain the low thermal conductance of the superlattice from experiments.

IV. CONCLUSION

In this paper, an integrated MD simulation and AGF approach have been developed to study phonon transmission across lattice-mismatched interfaces with atomic reconstruction. MD simulation was used to simulate the atomic reconstruction for lattice-mismatched interfaces. The recursive AGF approach was employed to calculate phonon transmission across lattice-mismatched interfaces with defects and species mixing, which addresses the numerical challenge in calculating phonon transmission for a relatively large cross-sectional area. Lattice mismatch increases the lattice disorder and decreases the adhesion energy, which in turn lowers phonon transmission and reduces the interface thermal conductance across lattice-mismatched interfaces. Further studies show that low-frequency phonons can be significantly scattered by increasing the defect size across the interface, while high-frequency phonons can be scattered almost completely (phonon transmission < 0.1) across an alloyed layer as small as 2.27 nm. The lattice-mismatch effects become smaller for interfaces with defects and species mixing. The effect of annealing temperature on the Si/Ge interface thermal conductance was studied. A significant reduction of the Si/Ge interface thermal conductance was observed for a lattice-mismatched interface when annealed at high temperature, which agrees well with the available experimental data in literature.

ACKNOWLEDGMENTS

The authors would like to thank their team members, Xiaokun Gu, Jun Liu, Dr. Jun Zhou, and Dr. Christopher J. Oshman, for proofreading and helpful comments on this paper. This work was partially supported by AFOSR Grant No. FA9550-08-1-0078, NSF CAREER Grant No. 0846561, and DARPA (Contract No. N66001-10-C-4002, managed by Dr. Thomas Kenny and Dr. Avi Bar-Cohen).

APPENDIX

The Tersoff empirical potential[35] is used in this paper for describing the atomic interaction in the Si/Ge and Si/Ge-like material system. The potential between atoms i and j can be expressed as

$$V_{ij} = f_c(r_{ij})[A_{ij}\exp(-\lambda_{ij}r_{ij}) - b_{ij}B_{ij}\exp(-\mu_{ij}r_{ij})], \tag{A1}$$

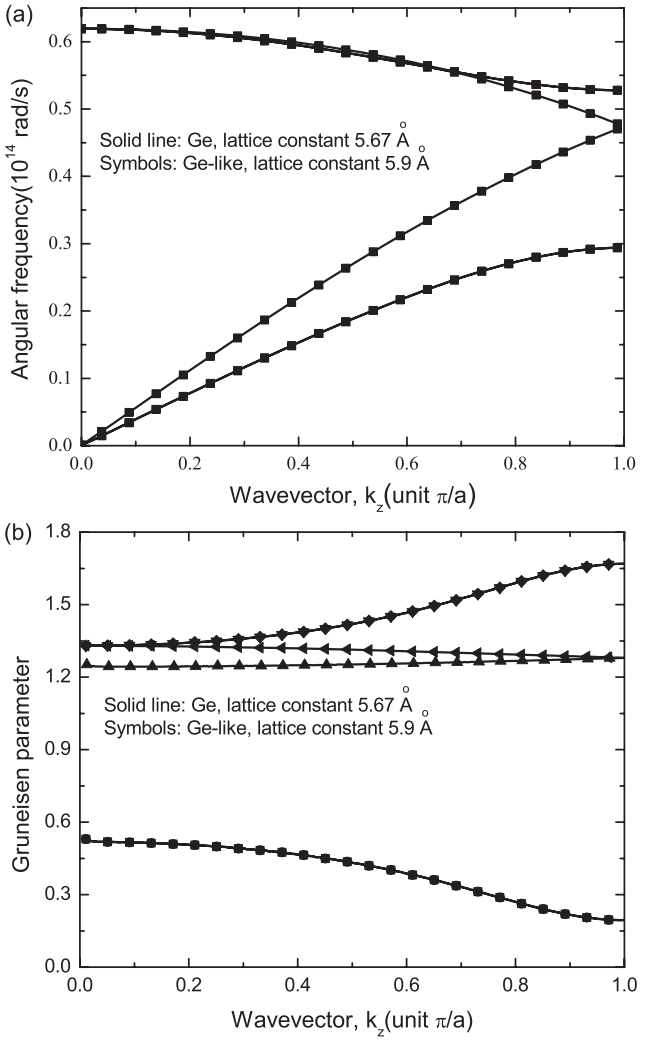

FIG. 10. (a) Phonon dispersion and (b) Grüneisen parameter of Ge with lattice constant of 5.67 Å and Ge-like material with lattice constant of 5.9 Å. The results show the new Ge-like material has the same phonon spectra as that in Ge.

where r_{ij} is the distance between atom i and j; $f_c(r_{ij})$ is a cutoff function; b_{ij} is a function related to the bond angle formed between i, j and the other neighboring atoms of atom i; and A, B, λ, and μ are parameters that can be found in Ref. 35. In our calculation, the Ge potential is modified to form Ge-like materials with different lattice constants so that we can examine the effect of different lattice-mismatch percentage on phonon transmission. The Ge-like materials with modified potential have the same phonon spectra as Ge. Since the Ge-like materials have the same crystal structure as Ge but with different lattice constants, the bond angles between any pair of atoms in the Ge-like materials are the same as those in Ge and no modification of the function of b_{ij} is needed. The other parameters for Ge-like materials can be derived from

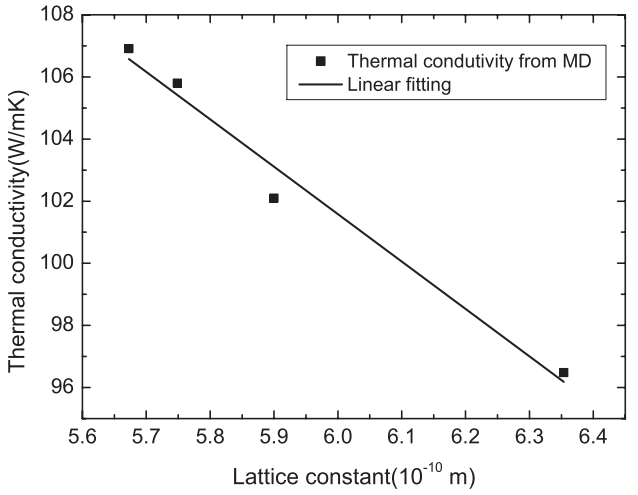

FIG. 11. Thermal conductivity of Ge-like materials with different lattice constants.

the following equations by comparing the second derivative of function V_{ij} over distance r_{ij}:

$$\lambda_{ij}{}' r_{ij}{}' = \lambda_{ij} r_{ij}, \quad \mu_{ij}{}' r_{ij}{}' = \mu_{ij} r_{ij}, \tag{A2}$$

$$A_{ij}{}' \lambda_{ij}{}'^2 = A_{ij} \lambda_{ij}{}^2, \quad B_{ij}{}' \lambda_{ij}{}'^2 = B_{ij} \lambda_{ij}{}^2, \tag{A3}$$

where $A_{ij}{}'$, $B_{ij}{}'$, $\lambda_{ij}{}'$, and $\mu_{ij}{}'$ are the parameters for the Ge-like materials. From Eq. (A2), the value of $\lambda_{ij}{}'$ and $\mu_{ij}{}'$ can be determined with the value of r_{ij} and $r_{ij}{}'$ taken from the lattice constants of Ge and Ge-like, respectively. Then from Eq. (A3), $A_{ij}{}'$ and $B_{ij}{}'$ can be determined. With the new parameters for Ge-like materials, the phonon dispersion and the Grüneisen parameter are calculated. For example, Fig. 10 shows the phonon dispersion and the Grüneisen parameter of Ge-like material with a lattice constant of 5.9 Å. Both phonon dispersion and the Grüneisen parameter of the Ge-like materials agree well with those of Ge.

However, the anharmonic force constants (third order and higher orders) could be different for the Ge and Ge-like materials. In Fig. 11, the thermal conductivity of Ge-like materials with different lattice constants is calculated using the spectral analysis[54] of the Green Kubo's relation from equilibrium molecular dynamics. Apparently, the thermal conductivity of Ge-like material is different from that of Ge, which indicates that the anharmonic force in the modified potential is different, although the phonon spectra are the same.

We note that the AGF simulations presented here are based on the harmonic approximation and only the harmonic force constant is used in the simulation. The anharmonic terms will not directly affect the phonon transmission results, but there is an effect through the structure change due to the difference in higher-order force constants. Considering this, these anharmonic terms would affect the result in a minor way compared with the harmonic terms.

*ronggui.yang@colorado.edu

[1]E. T. Swartz and R. O. Pohl, Rev. Mod. Phys. **61**, 605 (1989).

[2]D. G. Cahill, W. K. Ford, K. E. Goodson, G. D. Mahan, A. Majumdar, H. J. Maris, R. Merlin, and S. R. Phillpot, J. Appl. Phys. **93**, 793 (2003).

[3]G. Chen, D. Borca-Tasciuc, and R. G. Yang, Encycl. Nanosci. Nanotechnol. **7**, 429 (2004).
[4]Strictly speaking, it should be termed as local energy density when the local temperature cannot be defined at the interface.
[5]A. Maiti, G. D. Mahan, and S. T. Pantelides, Solid State Commun. **102**, 517 (1997).
[6]A. R. Abramson, C.-L. Tien, and A. Majumdar, J. Heat Transfer **124**, 963 (2002).
[7]Y. Chen, D. Li, J. Yang, Y. Wu, J. R. Lukes, and A. Majumdar, Physica B **349**, 270 (2004).
[8]R. J. Stevens, L. V. Zhigilei, and P. M. Norris, Int. J. Heat Mass Transf. **50**, 3977 (2007).
[9]M. Hu, P. Keblinski, and P. K. Schelling, Phys. Rev. B **79**, 104305 (2009).
[10]E. S. Landry and A. J. H. McGaughey, Phys. Rev. B **80**, 165304 (2009).
[11]S. Shin, M. Kaviany, T. Desai, and R. Bonner, Phys. Rev. B **82**, 081302 (2010).
[12]H.-B. Fan, K. Zhang, and M. M. F. Yuen, J. Appl. Phys. **106**, 034307 (2009).
[13]X. Huang, X. Wang, and B. Cook, J. Phys. Chem. C **114**, 21003 (2010).
[14]Z. Hassan, N. Allec, S. Li, R. P. Dick, V. Venkatraman, and Y. Ronggui, IEEE Trans. Comput.-Aided Des. **28**, 860 (2009).
[15]R. Yang and G. Chen, Phys. Rev. B **69**, 195316 (2004).
[16]R. Yang, G. Chen, and M. S. Dresselhaus, Phys. Rev. B **72**, 125418 (2005).
[17]R. Yang, G. Chen, M. Laroche, and Y. Taur, J. Heat Transfer **127**, 298 (2005).
[18]M.-S. Jeng, R. Yang, D. Song, and G. Chen, J. Heat Transfer **130**, 042410 (2008).
[19]P. Lee, K. Maute, and R. Yang, in *Multiscale Methods in Computational Mechanics*, Vol. 55 (Springer, New York, 2011), p. 195.
[20]L.-C. Liu, M.-J. Huang, R. Yang, M.-S. Jeng, and C.-C. Yang, J. Appl. Phys. **105**, 104313 (2009).
[21]W. Tian and R. Yang, Appl. Phys. Lett. **90**, 263105 (2007).
[22]L. G. C. Rego and G. Kirczenow, Phys. Rev. Lett. **81**, 232 (1998).
[23]P. K. Schelling, S. R. Phillpot, and P. Keblinski, Appl. Phys. Lett. **80**, 2484 (2002).
[24]R. J. Stoner, H. J. Maris, T. R. Anthony, and W. F. Banholzer, Phys. Rev. Lett. **68**, 1563 (1992).
[25]H. Zhao and J. B. Freund, J. Appl. Phys. **97**, 024903 (2005).
[26]W. Zhang, T. S. Fisher, and N. Mingo, Numer. Heat Transfer, Part B **51**, 333 (2007).
[27]W. Zhang, T. S. Fisher, and N. Mingo, J. Heat Transfer **129**, 483 (2007).
[28]Z. Huang, T. S. Fisher, and J. Y. Murthy, Journal article **109**, 074305 (2011).
[29]H. Zhao and J. B. Freund, J. Appl. Phys. **105**, 013515 (2009).
[30]X. Li and R. Yang, J. Phys.: Condens. Matter **24**, 155302 (2012).
[31]Z. Huang, J. Y. Murthy, and T. S. Fisher, J. Heat Transfer **133**, 114502 (2011).
[32]J. W. Jiang and J. S. Wang, Europhys. Lett. **96** (2011).
[33]S. Pettersson and G. D. Mahan, Phys. Rev. B **42**, 7386 (1990).
[34]W. Jian and W. Jian-Sheng, J. Phys.: Condens. Matter **19**, 236211 (2007).
[35]J. Tersoff, Phys. Rev. B **39**, 5566 (1989).
[36]L. J. Porter, S. Yip, M. Yamaguchi, H. Kaburaki, and M. Tang, J. Appl. Phys. **81**, 96 (1997).
[37]S. J. Cook and P. Clancy, Phys. Rev. B **47**, 7686 (1993).
[38]S. Datta, *Quantum Transport: Atom to Transistor* (Cambridge University Press, Cambridge, England, 2005).
[39]F. Guinea, C. Tejedor, F. Flores, and E. Louis, Phys. Rev. B **28**, 4397 (1983).
[40]D. K. Ferry, S. M. Goodnick, and J. Bird, *Transport in Nanostructures* (Cambridge University Press, New York, 2009).
[41]N. Mingo, in *Thermal Nanosystems and Nanomaterials*, edited by S. Volz, Vol. 118 (Springer-Verlag Berlin, 2009), p. 63.
[42]J.-S. Wang, J. Wang, and N. Zeng, Phys. Rev. B **74**, 033408 (2006).
[43]N. Mingo, Phys. Rev. B **74**, 125402 (2006).
[44]K. Esfarjani, G. Chen, and H. T. Stokes, Phys. Rev. B **84**, 085204 (2011).
[45]J. Shiomi, K. Esfarjani, and G. Chen, Phys. Rev. B **84**, 104302 (2011).
[46]A. Majumdar, J. Heat Transfer **115**, 7 (1993).
[47]H. Stohr and W. Klemm, Z. Anorg. Allg. Chem. **241**, 305 (1939).
[48]P. E. Hopkins, P. M. Norris, R. J. Stevens, T. E. Beechem, and S. Graham, J. Heat Transfer **130**, 062402 (2008).
[49]E. Bozorg-Grayeli, J. P. Reifenberg, M. A. Panzer, J. A. Rowlette, and K. E. Goodson, IEEE Electron Device Lett. **32**, 1281 (2011).
[50]S. M. Lee, D. G. Cahill, and R. Venkatasubramanian, Appl. Phys. Lett. **70**, 2957 (1997).
[51]T. Borca-Tasciuc, W. Liu, J. Liu, T. Zeng, D. W. Song, C. D. Moore, G. Chen, K. L. Wang, M. S. Goorsky, T. Radetic, R. Gronsky, T. Koga, and M. S. Dresselhaus, Superlattices Microstruct. **28**, 199 (2000).
[52]B. Yang and G. Chen, Phys. Rev. B **67**, 195311 (2003).
[53]S. Ethier and L. J. Lewis, J. Mater. Res. **7**, 2817 (1992).
[54]X. Li, K. Maute, M. L. Dunn, and R. Yang, Phys. Rev. B **81**, 245318 (2010).